Resonant wave formation in Bose-Einstein condensates

Alexandru I. Nicolin*
"Horia Hulubei" National Institute for Physics and Nuclear Engineering, 30 Reactorului, Magurele 077125, Romania
(Received 5 August 2011; revised manuscript received 10 October 2011; published 4 November 2011)

We investigate analytically the dynamics of a trapped, quasi-one-dimensional Bose-Einstein condensate subject to resonant and nonresonant periodic modulation of the transverse confinement. The dynamics of the condensate is described variationally through a set of coupled ordinary differential equations, and the period of the excited waves is determined analytically using a Mathieu-type analysis. For a modulation frequency equal to that of the radial confinement we show that the predicted period of the resonant wave is in agreement with the existing experimental results. Finally, we present a detailed comparison between the resonant waves and the Faraday waves that emerge outside of resonance.

DOI: 10.1103/PhysRevE.84.056202 PACS number(s): 05.45.−a, 03.75.Kk

I. INTRODUCTION

The dynamical properties of a driven Bose-Einstein condensate (BEC) go from purely quantum effects stemming from its superfluid nature to nonlinear effects that can be explained on classical grounds. Examples of such effects include the emergence of quantized vortices in stirred BECs for the former type [1] and a wide variety of nonlinear waves (such as shock waves, bright, dark, gap and vortex solitons, period doubled and fractional states, etc.) for the latter [2].

The interest in the parametric excitation of nonlinear waves in superfluids [3–5] has been substantially catalyzed by the experiments on Faraday waves in ^{87}Rb BECs [6] and ^{4}He cells [7], and those on the collective modes of a ^{7}Li BEC subject to periodic modulation of the scattering length [8]. Among the recent investigations we mention the study of resonances and the nonlinear correction to the frequencies of the collective modes of a BEC [9], the ultra-fast path-integral methods for the dynamics of quantum gases [10], the detailed analyses of Faraday patterns in superfluid Fermi gases [11,12] and trapped BECs [13–16], the removal of excitations in BECs subject to time-dependent periodic potentials [17], the parametric excitation of "scars" in BECs [18] and, finally, the spin-charge separation in one-dimensional fermionic systems [19]. On a related topic, the formation of density waves has been predicted for expanding condensates [20,21], and the spontaneous formation of density waves has been recently reported for antiferromagnetic ^{87}Rb BECs [22].

In this paper we investigate by variational means the dynamics of a trapped, cigar-shaped BEC subject to periodic modulation of the transverse confinement. It has been noted experimentally that the waves excited at a modulation frequency equal to that of the radial confinement have a period considerably smaller than that of the Faraday waves excited outside of resonance [6], while on the theoretical side the nonpolynomial Schrödinger equations [23] used to model Faraday waves were not able to capture the radial parametric resonance and, consequently, the emergence of the longitudinal resonant wave. Following the recent variational treatment of Faraday waves [24], we show that such a modulation of the transverse confinement turns unstable an otherwise stable longitudinal wave and has a minor influence on the Faraday wave. Using a Mathieu-type analysis on the equations that stem from the variational recipe, we determine analytically the period of the excited wave and show that it is in agreement with the experimental results [6].

The rest of the paper is structured as follows: In Sec. II we introduce the variational recipe and derive a set of coupled ordinary differential equations for the dynamics of the condensate. In Sec. III we introduce the Faraday and the resonant waves, and we determine the corresponding dispersion relations and show numerically that for a modulation frequency equal to that of the radial confinement the resonant wave is the most unstable. Finally, in the last section of the paper we present the concluding remarks along with some directions of future research.

II. VARIATIONAL TREATMENT

We build the variational equations starting from the Gross-Pitaevskii (GP) Lagrangian density (with $\hbar = m = 1$) of a cylindrically symmetric condensate [25], namely,

$$\mathcal{L}[\psi;r,z,t] = \frac{i}{2}\left(\psi\frac{\partial\psi^*}{\partial t} - \psi^*\frac{\partial\psi}{\partial t}\right) + \frac{1}{2}|\nabla\psi|^2 + V(\mathbf{r},t)\,|\psi|^2 + \frac{gN}{2}|\psi|^4, \tag{1}$$

where $r^2 = x^2 + y^2$, $\psi = \psi(\mathbf{r},t)$, $V(\mathbf{r},t) = 1/2\,\Omega^2(t)r^2$, g is proportional to the scattering length, and N is the number of bosons, using the hybrid trial wave function

$$\psi = f\,[k,w(t),u(t),v(t)]\exp\left[-\frac{r^2}{2w^2(t)} + ir^2\alpha(t)\right] \times\{1 + [u(t) + iv(t)]\cos kz\}, \tag{2}$$

where the normalization function is given by

$$f\,[k,w(t),u(t),v(t)] = \frac{1}{\pi\,w(t)}\sqrt{\frac{k}{2 + u^2(t) + v^2(t)}}. \tag{3}$$

The wave function accounts for the bulk part of the condensate through a radial Gaussian envelope of width $w(t)$ and incorporates a longitudinal surface wave of wave number k

*nicolin@theory.nipne.ro

grafted on the radial envelope. For the normalization we have used

$$\int_0^\infty \int_{-\pi/k}^{\pi/k} dr\, dz 2\pi r\, |\psi|^2 = 1. \tag{4}$$

To address more realistic experimental setups the ansatz can be refined to cover high-density condensates by using a q-Gaussian function for the radial envelope [26], and one can also incorporate a longitudinal external potential by grafting the corresponding envelope to the ansatz. These refinements, however, do not impact the mechanism behind the emergence of the resonant waves, and we shall neglect them for the moment. Computing the Lagrangian one has

$$\begin{aligned} L = {} & w^2(t)\dot{\alpha}(t) + \Omega^2(t)w^2(t) + \frac{1}{2w^2(t)} + 2w^4(t)\alpha^2(t) \\ & + \frac{k^2[u^2(t)+v^2(t)] + 2u(t)\dot{v}(t) - 2\dot{u}(t)v(t)}{2[2+u^2(t)+v^2(t)]} \\ & + \frac{8+3[u^2(t)+v^2(t)]^2 + 8v^2(t) + 24u^2(t)}{8\pi[2+u^2(t)+v^2(t)]^2 w^2(t)(\rho g)^{-1}}, \end{aligned} \tag{5}$$

where ρ represents the linear (longitudinal) density of the condensate and $L = L[w(t), \alpha(t), u(t), v(t); t]$. The first four terms of the Lagrangian describe the bulk of the condensate, while the last two represent the contribution of the surface wave. To cast the Euler-Lagrange equations

$$\frac{d}{dt}\left(\frac{\partial L}{\partial \dot{q}(t)}\right) = \frac{\partial L}{\partial q(t)}, \tag{6}$$

with $q(t) \in \{w(t), \alpha(t), u(t), v(t)\}$, in a simple form, we will restrict our analysis to small-amplitude surface waves, in which case we have

$$\dot{w}(t) = 2w(t)\alpha(t), \tag{7}$$

$$\dot{\alpha}(t) = -\frac{\Omega^2(t)}{2} + \frac{1}{2w^4(t)} + \frac{\rho g}{4\pi w^4(t)} - 2\alpha^2(t), \tag{8}$$

and

$$\dot{u}(t) = \frac{k^2 v(t)}{2}, \tag{9}$$

$$\dot{v}(t) = -\frac{k^2 u(t)}{2} - \frac{\rho g u(t)}{\pi w^2(t)}. \tag{10}$$

Equations (7) and (8) are well known and describe the dynamics of the bulk of the condensate, while Eqs. (9) and (10) describe the dynamics of the surface wave and resemble those derived in Refs. [15,27]. The main difference between Eqs. (9) and (10) and those derived in Refs. [15,27] is that the above equations stem from an energy minimization recipe and include the full impact of the radial dynamics on the surface wave [through the last term in Eq. (10)], while the equations derived in Refs. [15,27] appear after linearizing a perturbed ground state of a homogeneous cigar-shaped condensate and include the radial dynamics only in its lowest approximation; namely, the radial width is inversely proportional to the square root of the radial (time-modulated) trap frequency. This approximation of the dynamics of the radial width is intrinsic to nonpolynomial Schrödinger equations and prevents them from describing the formation of resonant waves.

Considering a drive of the form $\Omega(t) = \Omega(1 + \epsilon \sin \omega t)$ the previous equations can be conveniently recast as

$$\ddot{w}(\tau) = \frac{4}{\omega^2}\left[\frac{1}{w^3(\tau)} + \frac{\rho g}{2\pi w^3(\tau)} - \Omega^2(1+\epsilon\sin 2\tau)^2 w(\tau)\right], \tag{11}$$

$$\ddot{u}(\tau) = -\frac{2k^2}{\omega^2}\left[\frac{k^2}{2} + \frac{\rho g}{\pi w^2(\tau)}\right] u(\tau), \tag{12}$$

where $\omega t = 2\tau$. Equation (11) was originally introduced in 1880 by Ermakov [28], and it was later rediscovered several times (see Ref. [29] for a review). It is well known that it exhibits a series of parametric resonances at $\omega = 2\Omega, \Omega, \Omega/2, \ldots, 2\Omega/n^2$ [3], where n is a positive integer, whose characteristic curves, however, cannot be derived explicitly. For the rest of this paper we will focus only on the resonances at $\omega = 2\Omega$ and $\omega = \Omega$. The other resonances are outside of the frequency range used in the experiments on Faraday waves [6] and have substantially smaller widths.

III. RESULTS AND DISCUSSION

A. Nonresonant regime

In the nonresonant regime, namely, $\omega \neq \Omega$ and $\omega \neq 2\Omega$, one can disregard the second derivative of $w(\tau)$ in Eq. (11) and take

$$w(\tau) \approx \frac{1}{\sqrt{\Omega(1+\epsilon\sin 2\tau)}}\left(1 + \frac{\rho g}{2\pi}\right)^{1/4}, \tag{13}$$

which is identical with the approximation of the radial width considered in one-dimensional nonpolynomial Schrödinger equations [23], such that Eq. (12) yields

$$\frac{d^2u(\tau)}{d\tau^2} + [a(k,\omega) + b(k,\omega)\sin 2\tau]\, u(\tau) = 0, \tag{14}$$

where

$$a(k,\omega) = \frac{k^4}{\omega^2} + \frac{2\rho g k^2 \Omega}{\omega^2\sqrt{\pi^2 + \frac{\rho g \pi}{2}}}, \tag{15}$$

$$b(k,\omega) = \frac{2\epsilon\rho g k^2 \Omega}{\omega^2\sqrt{\pi^2 + \frac{\rho g \pi}{2}}}. \tag{16}$$

The surface waves observed experimentally correspond to the most unstable solutions of Eq. (14), and for small and positive values of $b(k,\omega)$ the dispersion relation of these solutions is given by $a(k,\omega) = 1$ [15]. To see this more clearly, we recall that (14) is a Mathieu equation, and according to the Floquet theory it has solutions of the form $u(\tau) = \exp(i\mu\tau)h(\tau)$, where, for small values of b, $h(\tau)$ is a linear combination of $\sin(\sqrt{a}\tau)$ and $\cos(\sqrt{a}\tau)$ [30]. The imaginary part of μ consists of a series of symmetrical lobes located at $a = n^2$, with n a positive integer, as depicted in Fig. 1. It is transparent from the figure that the most unstable solutions correspond to the lobe centered around $a = 1$, all the other ones being considerably smaller. For this lobe one has that

$$\mathrm{Im}[\mu] \approx -\frac{\sqrt{b^2(k,\omega) - 4\,[a(k,\omega)-1]^2}}{4}, \tag{17}$$

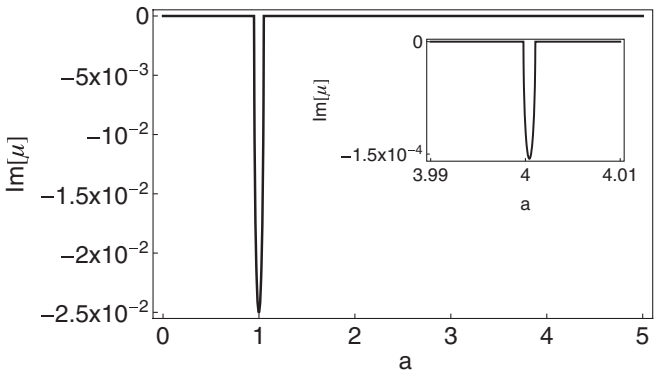

FIG. 1. Structure of Im[μ] of the solution of Eq. (14) for $b = 0.1$. Notice the large lobe centered around $a = 1$ and the substantially smaller one around $a = 2^2$. The other lobes (not shown) are centered around $a = n^2$, with n a positive integer larger than 2. These lobes are orders of magnitude smaller than the previous two and appear only above some (relatively large) critical values of b, being therefore irrelevant for the stability analysis of the surface waves.

where we have tacitly assumed that $b(k,\omega)$ is small. In honor of Faraday's classic study [31] on the behavior of "groups of particles (placed) upon vibrating elastic surfaces" and its much-celebrated appendix on the dynamics of "fluids in contact with vibrating surfaces," excited waves with a frequency half that of the drive are now called Faraday waves. In our case the dispersion relation of the Faraday waves is given by

$$k_F = \sqrt{\frac{\sqrt{2\rho^2 g^2\Omega^2 + \pi\omega^2(2\pi+\rho g)} - \sqrt{2}\rho g\Omega}{\sqrt{2\pi^2+\pi\rho g}}}, \qquad (18)$$

and the corresponding period is in agreement with the experimental results in Ref. [6]. Finally, let us notice that Eqs. (17) and (18) indicate that Faraday waves emerge slower at higher driving frequencies as

$$\mathrm{Im}[\mu_F] \sim -\frac{\epsilon g\rho\Omega}{\omega^2(2\pi+g\rho)}[\omega^2\pi(2\pi+g\rho) + 4g^2\Omega^2\rho^2 - 2g\Omega\rho\sqrt{4g^2\Omega^2\rho^2 + 2\omega^2(2\pi+g\rho)}]^{1/2}. \qquad (19)$$

B. Resonant regime

In the vicinity of the first resonance, namely, $\omega \approx \Omega$, the higher harmonics in $1/w^2(\tau)$ can no longer be disregarded (as in the approximation used far from resonance), and the excited waves are therefore no longer governed by a Mathieu equation. For the dispersion relation, however, we will neglect the impact of these higher harmonics and will use $a(k,\omega)$ defined in Eq. (15).

Let us first notice that due to the resonant behavior $a(k,\omega) = 1$ does not correspond anymore to the most unstable solutions. In fact, the instability now emerges due to the resonant energy transfer between $w(\tau)$ and $u(\tau)$, which sets $a(k,\omega) = 2^2$ such that (unlike the nonresonant regime) $w(\tau)$ and $u(\tau)$ oscillate on the same frequency. The dispersion

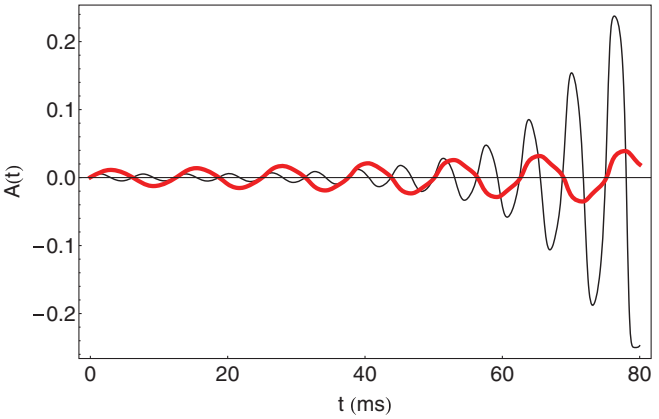

FIG. 2. (Color online) The emergence of the resonant and the Faraday wave at $\omega = \Omega$ for a realistic experimental setup consisting of a condensate of $N = 5 \times 10^5$ atoms extending over 180 μm, $\epsilon = 0.1$, and a magnetic trap with a radial frequency $\Omega = 160.5(2\pi)$ Hz. The thin black line corresponds to the $A(t)$ amplitude of the resonant wave, and the full red line corresponds to the $A(t)$ amplitude of the Faraday wave. Notice that the Faraday wave has a frequency half that of the resonant wave.

relation of the resonant waves is then given by

$$k_R = \sqrt{\frac{\sqrt{\rho^2 g^2\Omega^2 + 2\pi\omega^2(2\pi+\rho g)} - \rho g\Omega}{\sqrt{\pi^2+\pi\rho g/2}}}. \qquad (20)$$

To see more clearly the resonant dynamics of the condensate, we compare in Fig. 2 the emergence of the resonant and the Faraday wave at $\omega = \Omega$ in a realistic experimental setup consisting of $N = 5 \times 10^5$ ^{87}Rb atoms extending over 180 μm, $\epsilon = 0.1$ and a magnetic trap with $\Omega = 160.5(2\pi)$ Hz [32]. The numerical solutions of Eqs. (11) and (12) [with k given by Eq. (18) for the Faraday wave and by Eq. (20) for the resonant wave] provide the longitudinal profile of the condensate, namely,

$$\phi(z,t) = \int_0^\infty dr 2\pi r\,|\psi|^2\,, \qquad (21)$$

that we use to compute the amplitude of the wave

$$\phi(0,t) - \phi\left(\frac{\pi}{k},t\right) = \frac{4ku(t)}{\pi[2+u^2(t)+v^2(t)]}. \qquad (22)$$

The $4k/\pi$ factor can be disregarded as it plays no role in the dynamics, and one can monitor the emergence of the instability by looking at the function

$$A(t) = \frac{u(t)}{2+u^2(t)+v^2(t)} \qquad (23)$$

for each wave under scrutiny. As one can clearly see from Fig. 2, the resonant wave emerges faster than the Faraday wave and shows the exponential growth typical for resonant forcing. In the absence of the drive the resonant wave shows very weak signs of numerical instability.

In the vicinity of the second resonance, namely, $\omega \approx 2\Omega$, the resonant wave emerges slower than the Faraday wave and is therefore not observed experimentally. To see this, we plot in Fig. 3 the numerical solution of Eqs. (11) and (12) at $\omega = 2\Omega$

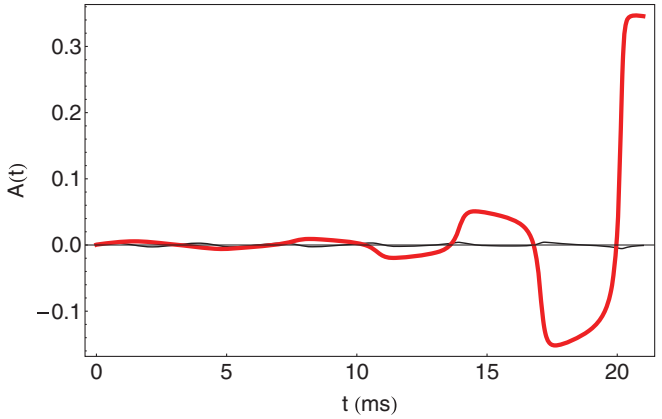

FIG. 3. (Color online) The emergence of the resonant and the Faraday wave at $\omega = 2\Omega$ for an experimental setup identical to that considered in Fig. 2. The thin black line corresponds to the $A(t)$ amplitude of the resonant wave, and the full red line corresponds to the $A(t)$ amplitude of the Faraday wave. Notice that the Faraday wave has a frequency half that of the resonant wave.

for the two waves, using Eq. (18) for the dispersion of the Faraday wave and Eq. (20) for the dispersion of the resonant wave. As this resonance is considerably wider than that at $\omega = \Omega$ [3] and we have seen that outside of resonances Faraday waves emerge slower at higher values of ω, one could naively expect the opposite situation. A close inspection, however, of $w(t)$ shown in Fig. 4 reveals the strong contribution of the higher harmonics responsible for the "bouncing ball" behavior. This means that close to $\omega = 2\Omega$ Eqs. (9) and (10) do not yield a Mathieu equation, and, consequently, the approximation of Im[μ] fails. In fact, $u(\tau)$ is now governed by a general Hill equation, namely,

$$\ddot{u}(\tau) + [a + b\sin 2\tau + c\sin 4\tau + d\sin 8\tau \cdots]\, u(\tau) = 0, \quad (24)$$

for which no analytic approximation of the Floquet exponent is known.

Using Eq. (20) one has that at $\omega = \Omega$ the period of the resonant wave is around 12.4 μm. The experimental results indicate that close to resonance the surface wave has a

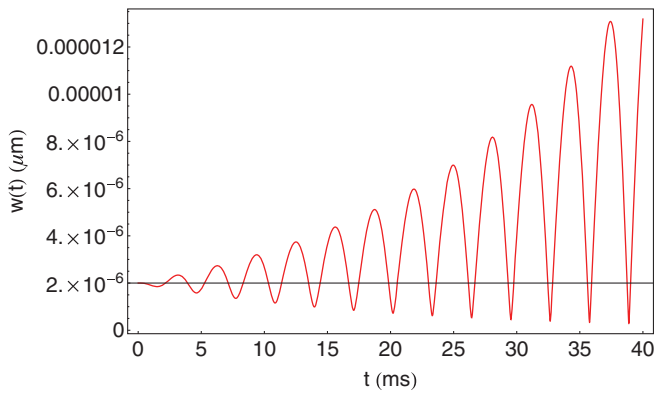

FIG. 4. (Color online) The dynamics of $w(t)$ at $\omega = 2\Omega$ for an experimental setup identical to that considered in Fig. 2. The red line represents $w(t)$, and the black line shows the equilibrium value of the width.

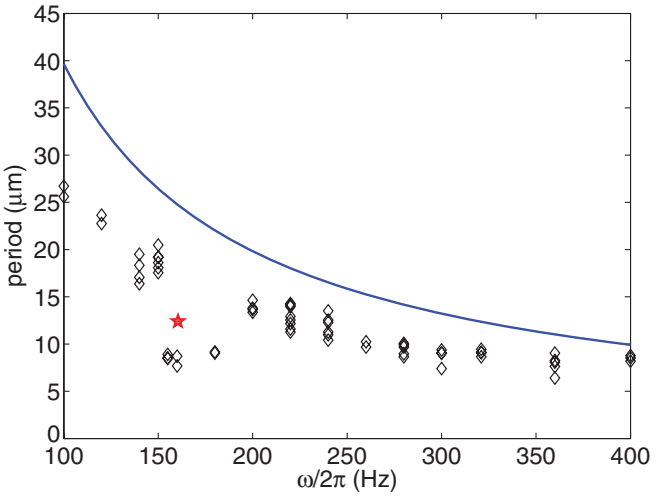

FIG. 5. (Color online) The period of the surface waves excited in cigar-shaped BEC through periodic modulations of the radial component of the confining potential. The black diamonds correspond to the experimental data in Ref. [6], the full blue curve corresponds to the Faraday waves defined by Eq. (18), and the red pentagram represents the current prediction for the period of the resonant wave.

period between 7.68 and 9.17 μm, which is in qualitative agreement with our result given that the variational calculation consistently overestimates the period of the observed surface waves, as one can see in Fig. 5. Note that the instability onset time of the resonant wave increases with the distance from the resonance, therefore the rather scattered experimental data just before the first resonance could signal the superposition of a Faraday and a resonant wave. At $\omega = 2\Omega$ Eq. (20) indicates a period of around 6.2 μm, but the resonant wave cannot be seen experimentally as it emerges slower than the Faraday wave.

To address directly the experimental results reported in Ref. [6] for $\omega = \Omega$, we incorporate a weak longitudinal potential in the GP Lagrangian density and graft the corresponding envelope to the ansatz, that is,

$$\psi = f[\cdots]\exp\left\{\sum_{j=r,z}\left[-\frac{j^2}{2w_j^2(t)} + ij^2\alpha_j(t)\right]\right\} \times \{1 + [u(t) + iv(t)]\cos kz\}, \quad (25)$$

where the normalization function $f[\cdots]$ is such that $\int d\mathbf{r}\,|\psi|^2 = 1$. Under the (experimentally correct) assumption that the period of the resonant wave is much smaller than the longitudinal width of the condensate, the Lagrangian is amenable to analytical manipulations, and one can derive the corresponding variational equations [24]. For waves of small amplitude they take the form

$$\dot{w}_j(t) = 2w_j(t)\alpha_j(t), \quad (26)$$

$$\dot{\alpha}_j(t) = \frac{1}{2w_j^4(t)} - \frac{\Omega_j^2}{2} + \frac{\tilde{N}g}{w_j^m(t)w_l^n(t)} - 2\alpha_j^2(t), \quad (27)$$

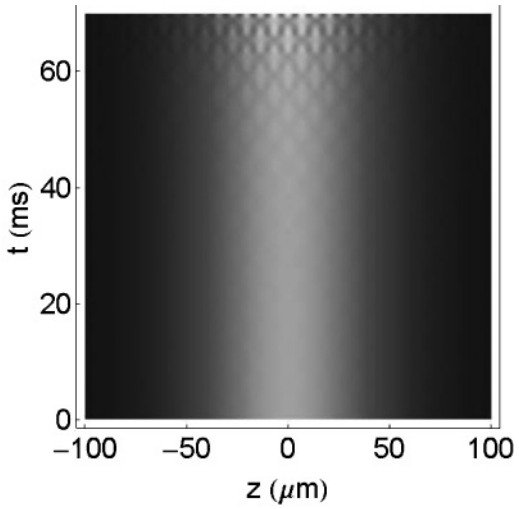

FIG. 6. The emergence of the resonant wave at $\omega = \Omega$ for the experimental conditions in Ref. [6] with $\epsilon = 0.1$. The bright regions of the density profile are the ones with the most number of atoms.

and

$$\dot{v}(t) = -u(t)\left[\frac{k^2}{2} + \frac{Ng}{\sqrt{2}\pi^{3/2}w_r^2(t)w_z(t)}\right], \tag{28}$$

$$\dot{u}(t) = \frac{k^2}{2}v(t), \tag{29}$$

where $j \in \{z,r\}, l \in \{r,z\}, m \in \{2,4\}, n \in \{3,1\}$, and $\tilde{N} = N/4\sqrt{2}\pi^{3/2}$. As in the case of a longitudinally homogeneous condensate k is determined such that close to equilibrium $u(t)$ and $w_r(t)$ oscillate on the same frequency. Using these equations we reconstruct in Fig. 6 the dynamics of $\phi(z,t)$ and show the emergence of the resonant wave for the experimental conditions in Ref. [6].

Finally, let us notice that for a trapping potential of constant strength and a scattering length modulated such that $g(t) = g(1 + \epsilon \sin \omega t)$, we can use Eqs. (26) and (27) to study the emergence of surface waves through longitudinal resonances. To this end, one can show that outside of radial resonances

$$\ddot{w}_z(t) = -\Omega_z^2 w_z(t) + \frac{1}{w_z^3(t)} + \frac{g(t)N\Omega_r\pi^{-3/4}w_z^{-3/2}(t)}{\sqrt{2^{3/2}g(t)N + 8\pi^{3/2}w_z(t)}} \tag{30}$$

and

$$\ddot{u}(t) = \frac{k^2u(t)}{4}\left[-k^2 - \frac{2^{3/2}g(t)N\Omega_r\pi^{-3/4}w_z^{-1/2}(t)}{\sqrt{2^{3/2}g(t)N + 8\pi^{3/2}w_z(t)}}\right], \tag{31}$$

which can be easily solved numerically. Such longitudinal resonances could be seen for small values of ϵ in experimental setups similar to that in Ref. [8].

IV. CONCLUSIONS

We have presented a variational treatment for the dynamics of surface waves in BECs with longitudinal homogeneity, and have shown that for condensates subject to periodic modulation of the transverse confinement on a frequency equal to that of the radial confinement the excited surface wave is distinct from the Faraday waves that emerge outside of resonance. The period of this resonant wave has been determined analytically using a Mathieu-type analysis, and we have compared numerically our theoretical results with the available experimental data to illustrate the agreement.

Extending the variational treatment of surface waves to address the recently reported condensate fragmentation [8] is still an open problem, as is the management of surface waves through the joint modulation of the scattering length and the radial component of the magnetic trap. Also on the side of future research topics we mention the dynamics of surface waves in dissipative BECs, especially the coupling of a surface wave to the thermal component of the cloud, and the formation of resonant waves in binary condensates.

ACKNOWLEDGMENTS

The author thanks Dumitru Mihalache, Aurelian Isar, Mihaela-Carina Rapotaru, Mihai Gîrţu, and Antun Balaž for insightful discussions, and is grateful to Peter Engels for communicating the experimental data in Ref. [6]. This work was supported by CNCS-UEFISCDI through the postdoctoral grant PD122 contract no. 35/28.07.2010. Part of this work was done during a research stage at Ovidius University, Constanţa.

[1] C. J. Pethick and H. Smith, *Bose-Einstein Condensation in Dilute Gases* (Cambridge University Press, Cambridge, 2008).

[2] P. G. Kevrekidis, D. J. Frantzeskakis, and R. Carretero-González (eds.), *Emergent Nonlinear Phenomena in Bose-Einstein Condensates* (Springer-Verlag, Berlin, 2008); R. Carretero-González, D. J. Frantzeskakis, and P. G. Kevrekidis, Nonlinearity **21**, R139 (2008); D. J. Frantzeskakis, J. Phys. A: Math. Theor. **43**, 213001 (2010); Y. V. Kartashov, B. A. Malomed, and L. Torner, Rev. Mod. Phys. **83**, 247 (2011).

[3] J. J. García-Ripoll, V. M. Pérez-García, and P. Torres, Phys. Rev. Lett. **83**, 1715 (1999).

[4] K. Staliunas, S. Longhi, and G. J. de Valcárcel, Phys. Rev. Lett. **89**, 210406 (2002); Phys. Rev. A **70**, 011601(R) (2004).

[5] M. Modugno, C. Tozzo, and F. Dalfovo, Phys. Rev. A **74**, 061601(R) (2006).

[6] P. Engels, C. Atherton, and M. A. Hoefer, Phys. Rev. Lett. **98**, 095301 (2007).

[7] H. Abe, T. Ueda, M. Morikawa, Y. Saitoh, R. Nomura, and Y. Okuda, Phys. Rev. E **76**, 046305 (2007); T. Ueda, H. Abe, Y. Saitoh, R. Nomura, and Y. Okuda, J. Low Temp. Phys. **148**, 553 (2007).

[8] S. E. Pollack, D. Dries, R. G. Hulet, K. M. F. Magalhaes, E. A. L. Henn, E. R. F. Ramos, M. A. Caracanhas, and V. S. Bagnato, Phys. Rev. A **81**, 053627 (2010).
[9] I. Vidanović, A. Balaž, H. Al-Jibbouri, and A. Pelster, Phys. Rev. A **84**, 013618 (2011).
[10] A. Balaž, A. Bogojević, I. Vidanović, and A. Pelster, Phys. Rev. E **79**, 036701 (2009); A. Balaž, I. Vidanović, A. Bogojević, A. Belić, and A. Pelster, J. Stat. Mech. (2011) P03004; (2011) P03005.
[11] P. Capuzzi and P. Vignolo, Phys. Rev. A **78**, 043613 (2008).
[12] R. A. Tang, H. C. Li, and J. K. Xue, J. Phys. B **44**, 115303 (2011).
[13] A. B. Bhattacherjee, Phys. Scr. **78**, 045009 (2008).
[14] P. Capuzzi, M. Gattobigio, and P. Vignolo, Phys. Rev. A **83**, 013603 (2011).
[15] A. I. Nicolin and M. C. Raportaru, Physica A **389**, 4663 (2010).
[16] R. Nath and L. Santos, Phys. Rev. A **81**, 033626 (2010).
[17] K. Staliunas, Phys. Rev. A **84**, 013626 (2011).
[18] N. Katz and O. Agam, New J. Phys. **12**, 073020 (2010).
[19] C. D. Graf, G. Weick, and E. Mariani, Europhys. Lett. **89**, 40005 (2010).
[20] L. Salasnich, N. Manini, F. Bonelli, M. Korbman, and A. Parola, Phys. Rev. A **75**, 043616 (2007).
[21] A. Imambekov, I. E. Mazets, D. S. Petrov, V. Gritsev, S. Manz, S. Hofferberth, T. Schumm, E. Demler, and J. Schmiedmayer, Phys. Rev. A **80**, 033604 (2009).
[22] J. Kronjäger, C. Becker, P. Soltan-Panahi, K. Bongs, and K. Sengstock, Phys. Rev. Lett. **105**, 090402 (2010).
[23] L. Salasnich, A. Parola, and L. Reatto, Phys. Rev. A **65**, 043614 (2002); L. Salasnich, Laser Phys. **12**, 198 (2002); J. Phys. A: Math. Theor. **42**, 335205 (2009); A. I. Nicolin, Rom. Rep. Phys. **61**, 641 (2009).
[24] A. I. Nicolin, Rom. Rep. Phys. **63**, 1329 (2011); A. I. Nicolin and M. C. Raportaru, Proc. Romanian Acad. A **12**, 209 (2011); A similar variational ansatz has been used to investigate the dynamics of loosely bound two-dimensional solitons in BECs loaded into optical lattices in A. Gubeskys, B. A. Malomed, and I. M. Merhasin, Stud. Appl. Math. **115**, 255 (2005).
[25] See, for instance, V. M. Pérez-García, H. Michinel, J. I. Cirac, M. Lewenstein, and P. Zoller, Phys. Rev. A **56**, 1424 (1997) for the dynamics of a condensate in a magnetic trap; see also A. I. Nicolin, Rom. Rep. Phys. **63**, 187 (2011) for the band structure of a condensate loaded into a longitudinal optical lattice.
[26] A. I. Nicolin and R. Carretero-Gonzáles, Physica A **387**, 6032 (2008).
[27] A. I. Nicolin, R. Carretero-González, and P. G. Kevrekidis, Phys. Rev. A **76**, 063609 (2007).
[28] V. Ermakov, Univ. Izv. Kiev **20**, 1 (1880).
[29] J. L. Reid and J. R. Ray, Z. Angew. Math. Mech. **64**, 365 (1984).
[30] N. W. McLachlan, *Theory and Application of Mathieu Functions* (Oxford University Press, New York, 1951).
[31] M. Faraday, Philos. Trans. R. Soc. London **121**, 299 (1831).
[32] The experimental setup considered here is similar to that used in Ref. [6] and describes quantitatively the observed Faraday waves. Due to the large number of atoms the spatial extent of the condensate is computed using a Thomas-Fermi density profile.